frontiers in Genetics

ORIGINAL RESEARCH
published: 24 March 2022
doi: 10.3389/fgene.2022.833083

16p12.1 Deletion Orthologs are Expressed in Motile Neural Crest Cells and are Important for Regulating Craniofacial Development in *Xenopus laevis*

Micaela Lasser[1], *Jessica Bolduc*[1], *Luke Murphy*[1], *Caroline O'Brien*[1], *Sangmook Lee*[1], *Santhosh Girirajan*[2] *and Laura Anne Lowery*[3]*

[1]Department of Biology, Boston College, Chestnut Hill, MA, United States, [2]Department of Biochemistry and Molecular Biology, Pennsylvania State University, State College, PA, United States, [3]Alfred B. Nobel Section of Hematology and Medical Oncology, Boston University School of Medicine and Boston Medical Center, Boston, MA, United States

OPEN ACCESS

Edited by:
Lucas Alvizi,
University of São Paulo, Brazil

Reviewed by:
Sumantra Chatterjee,
NYU Grossman School of Medicine, United States
Alex Star Nord,
University of California, Davis, United States

***Correspondence:**
Laura Anne Lowery
lalowery@bu.edu

Specialty section:
This article was submitted to Genetics of Common and Rare Diseases, a section of the journal Frontiers in Genetics

Received: *10 December 2021*
Accepted: *09 March 2022*
Published: *24 March 2022*

Citation:
Lasser M, Bolduc J, Murphy L, O'Brien C, Lee S, Girirajan S and Lowery LA (2022) 16p12.1 Deletion Orthologs are Expressed in Motile Neural Crest Cells and are Important for Regulating Craniofacial Development in Xenopus laevis. Front. Genet. 13:833083. doi: 10.3389/fgene.2022.833083

Copy number variants (CNVs) associated with neurodevelopmental disorders are characterized by extensive phenotypic heterogeneity. In particular, one CNV was identified in a subset of children clinically diagnosed with intellectual disabilities (ID) that results in a hemizygous deletion of multiple genes at chromosome 16p12.1. In addition to ID, individuals with this deletion display a variety of symptoms including microcephaly, seizures, cardiac defects, and growth retardation. Moreover, patients also manifest severe craniofacial abnormalities, such as micrognathia, cartilage malformation of the ears and nose, and facial asymmetries; however, the function of the genes within the 16p12.1 region have not been studied in the context of vertebrate craniofacial development. The craniofacial tissues affected in patients with this deletion all derive from the same embryonic precursor, the cranial neural crest, leading to the hypothesis that one or more of the 16p12.1 genes may be involved in regulating neural crest cell (NCC)-related processes. To examine this, we characterized the developmental role of the 16p12.1-affected gene orthologs, *polr3e*, *mosmo*, *uqcrc2*, and *cdr2*, during craniofacial morphogenesis in the vertebrate model system, *Xenopus laevis*. While the currently-known cellular functions of these genes are diverse, we find that they share similar expression patterns along the neural tube, pharyngeal arches, and later craniofacial structures. As these genes show co-expression in the pharyngeal arches where NCCs reside, we sought to elucidate the effect of individual gene depletion on craniofacial development and NCC migration. We find that reduction of several 16p12.1 genes significantly disrupts craniofacial and cartilage formation, pharyngeal arch migration, as well as NCC specification and motility. Thus, we have determined that some of these genes play an essential role during vertebrate craniofacial patterning by regulating specific processes during NCC development, which may be an underlying mechanism contributing to the craniofacial defects associated with the 16p12.1 deletion.

Keywords: 16p12.1 deletion, *Xenopus*, development, craniofacial, Neural Crest Cells (NCCs)

INTRODUCTION

Embryonic development requires the proper function of thousands of genes in order for cells to proliferate and divide, differentiate, migrate long distances to their final destination, and communicate with one another appropriately. Disruption of protein function due to mutations of genes that are required for these processes during embryogenesis can lead to severe developmental defects and neurodevelopmental disorders such as intellectual disabilities (ID) or Autism spectrum disorder (ASD) (Alonso-Gonzalez et al., 2018; Lasser et al., 2018; Chen et al., 2019; Kasherman et al., 2020; Sierra-Arregui et al., 2020). Genetic mutations caused by rare copy number variants (CNVs), including deletions and duplications, have been associated with neurodevelopmental disorders to varying degrees (Blazejewski et al., 2018; Deshpande and Weiss, 2018; Jensen et al., 2018; Pizzo et al., 2019; Rylaarsdam and Guemez-Gamboa, 2019; Singh et al., 2020). Recently, a CNV was identified in children diagnosed with ID, that results in a hemizygous deletion of several genes located at chromosome 16p12.1 (Antonacci et al., 2010; Girirajan et al., 2010). Individuals with this variant display phenotypic variability, presenting with a wide range of defects including microcephaly, seizures, cardiac defects, and growth retardation. Additionally, patients manifest severe craniofacial abnormalities including facial asymmetries, micrognathia (undersized jaw), a short philtrum (space between the nose and lip), as well as cartilage malformation of the ears and nose.

Craniofacial defects are one of the most prevalent congenital defects that can severely affect quality of life (Trainor, 2010; Kirby, 2017; Vega-Lopez et al., 2018). As craniofacial patterning relies heavily on the specification, proliferation, and subsequent migration of neural crest cells (NCCs), many craniofacial and cartilage defects arise due to aberrant NCC development (Trainor, 2010; Fish, 2016; Rutherford and Lowery, 2016; Vega-Lopez et al., 2018). Several of the tissue and organ systems affected by the 16p12.1 deletion are derived from NCCs; however, the function of the genes within this region have not been investigated in the context of vertebrate craniofacial development, nor has any study determined whether their depletion might impact NCC behavior. Therefore, the underlying developmental mechanism by which each gene contributes to the craniofacial phenotypes associated with the deletion remains to be elucidated.

The multigenic nature of the 16p12.1 deletion adds complexity to our understanding of the etiology behind this variant, due in part to the functional diversity of the affected genes. The 16p12.1 deletion encompasses a 520-kb region on the short arm of chromosome 16 and impacts several genes including *POLR3E*, *MOSMO*, *UQCRC2*, and *CDR2* (Antonacci et al., 2010; Girirajan et al., 2010). (While *EEF2K* and *VWA3A* are also in the 16p12.1 deletion region, in this study, we focus on the first four genes mentioned as they are all fully annotated in *Xenopus laevis* and are at least 70% conserved to the human ortholog of each gene.) RNA polymerase III subunit E (POLR3E) is important for catalyzing the transcription of small RNAs, though the exact function of *POLR3E* in relation to RNA polymerase III activity is unknown (Hu et al., 2002). Modulator of smoothened (*MOSMO*) is a negative regulator of Sonic Hedgehog (Shh) signaling by participating in the degradation of the Frizzled Class receptor, Smoothened (Pusapati et al., 2018). Additionally, reduced dosage of *polr3e* and *mosmo* were found to severely impact proper brain development in both *Drosophila melanogaster* and *Xenopus laevis*, suggesting that they may contribute to the ID and microcephaly phenotypes observed in patients with the 16p12.1 deletion (Pizzo et al., 2021). Ubiquinol-cytochrome C reductase core protein 2 (*UQCRC2*) is a component of the mitochondrial respiratory chain complex and is essential for the production of ATP (Miyake et al., 2013; Gaignard et al., 2017; Shang et al., 2018; Shan et al., 2019). Cerebellar degeneration related protein 2 (*CDR2*) is an onconeural protein that is known to be ectopically expressed in breast or ovarian tumors, resulting in the generation of autoantibodies that leads to cerebellar degeneration (Schubert et al., 2014; Hwang et al., 2016).

Due to the broad range of cellular functions of each 16p12.1-affected gene, it is imperative to determine whether their individual depletion leads to specific craniofacial defects, or whether depletion of multiple genes within this region combinatorially contributes to a collaborative craniofacial phenotype. Thus, we investigated the contributions of *polr3e*, *mosmo*, *uqcrc2*, and *cdr2* to developmental processes that govern early craniofacial patterning in *Xenopus laevis*. First, we examined expression profiles for each transcript across early stages of embryonic development, and we observed their expression in motile NCCs residing in the pharyngeal arches (PAs), suggesting that they may influence NCC development and migration. Knockdown (KD) strategies were then utilized to assess the contribution of each 16p12.1-affected gene to facial and cartilage development. We previously showed that depletion of *polr3e*, *mosmo*, and *uqcrc2* led to smaller facial features (Pizzo et al., 2021), and in the present study, we found that knockdown of these three genes also disrupt cartilage morphology. We then performed both *in vivo* and *in vitro* NCC migration assays, observing that some of these gene mutations also impact NCC migration in the pharyngeal arches and NCC motility rates. Finally, we examined NCC specification and proliferation, and while we found that reduced dosage of each gene did not have a significant impact on proliferation in our assay, we found that some of these genes are critical for NCC specification. Together, our results support the hypothesis that the craniofacial phenotypes associated with the 16p12.1 deletion are, in part, due to several genes within this region performing critical functions during NCC development and migration, craniofacial patterning, and cartilaginous tissue formation. Moreover, this work is the first to elucidate the roles of the 16p12.1-affected genes during embryonic craniofacial morphogenesis on a shared, directly-comparable genetic background, providing deeper insight into how diverse

genetic mutations lead to distinct developmental phenotypes and disease within the context of a multigenic syndrome.

MATERIALS AND METHODS

Xenopus Husbandry

Eggs obtained from female *Xenopus laevis* were fertilized *in vitro*, dejellied and cultured at 14-23°C in 0.1X Marc's modified Ringer's (MMR) using standard methods (Sive et al., 2010). Embryos received injections of exogenous mRNAs or antisense oligonucleotide strategies at the two or four cell stage, using four total injections performed in 0.1X MMR media containing 5% Ficoll. Embryos were staged according to Nieuwkoop and Faber (Nieuwkoop and Faber, 1994). All experiments were approved by the Boston College and Boston University Institutional Animal Care and Use Committees and were performed according to national regulatory standards.

Depletion and Rescue

Morpholinos (MOs) were targeted to early splice sites of *X. laevis mosmo* (for L, 5-ACAATTGACATCCACTTACTGCCGG-3; for S, 5- CACCTTCCCTACCCCGCTACTTAC-3), *polr3e* (for L, 5-ACTGTAAGCCTCTTTTGCCTTACCT-3), *uqcrc2* (for L, 5-ACAGTGTCTCTAAAGCACAGATACA-3; for S, 5-CCCCTAACCCATTAAACATATACCT-3), *cdr2* (for L and S, 5-CATCCCTCCCATACACTCACCTTG-3), or standard control MO (5-cctcttacctcagttacaatttata-3); purchased from Gene Tools (Philomath, OR). In knockdown (KD) experiments, all MOs were injected at either the 2-cell or 4-cell stage with embryos receiving injections 2 or 4 times total. *Mosmo* and control MOs were injected at 12ng/embryo for 50% KD and 20ng/embryo for 80% KD; *polr3e* and control MOs were injected at 5ng/embryo for 30% KD, 10ng/embryo for 50% KD and 20ng/embryo for 80% KD; *uqcrc2* and control MOs were injected at 35ng/embryo for 50% KD and 50ng/embryo for 80% KD; *cdr2* and control MOs were injected at 10 ng/embryo for 50% KD. Splice site MOs were previously validated through a Reverse transcriptase polymerase Chain Reaction (RT-PCR), as described (**Supplementary Figure S1**) (Pizzo et al., 2021). RNA was extracted from 10 two-day old whole embryos for each RT-PCR reaction.

Rescues were performed with exogenous mRNAs co-injected with their corresponding MO strategies (**Supplementary Figure S2**) (Pizzo et al., 2021). *Xenopus* ORFs for *mosmo*, *polr3e*, and *uqcrc2* were purchased from the European *Xenopus* Resource Center (EXRC) and gateway-cloned into pCSF107mT-GATEWAY-3′GFP destination vectors. Constructs used were *mosmo-gfp*, *polr3e-gfp*, *uqcrc2-gfp*, *cdr2-gfp*, and *gfp* in pCS2+. In rescue experiments, MOs were injected with mRNA (1,500 pg/embryo for *mosmo-gfp*; 2,000 pg/embryo for *polr3e-gfp*; 1000pg/embryo for *uqcrc2-gfp*; 1000pg/embryo for *cdr2-gfp*, and 300 pg/embryo for *gfp*) in the same injection solution.

Whole-Mount RNA *in situ* Hybridization

Embryos were fixed overnight at 4°C in a solution of 4% paraformaldehyde in PBS, gradually dehydrated in ascending concentration of methanol in PBS, and stored in methanol at−20°C for a minimum of 2 hours, before *in situ* hybridization, performed as previously described (Sive et al., 2007). After brief proteinase K treatment, embryos were bleached under a fluorescent light in a solution of 1.8x saline-sodium citrate, 1.5% H_2O_2, and 5% (vol/vol) formamide for 20–45 min before prehybridization. During hybridization, probe concentration was 0.5ug/mL.

The *Xenopus sox9* hybridization probe was a kind gift from Dr. Dominique Alfandari (University of Massachusetts at Amherst, MA, United States), and the *Xenopus twist* hybridization probe was a kind gift from Dr. Richard Harland and Dr. Helen Willsey (University of California Berkeley and University of California SF, CA, United States). The templates for making antisense probes for *polr3e*, *mosmo*, *uqcrc2*, and *cdr2* were PCR amplified from the reverse transcribed cDNA library, using the following primer sets: *polr3e* forward, 5′—GGATAGTCGCTCAGAACACG—3′, *polr3e* reverse, 5′—GGGTCAGCTTTGTCTGGATC—3′, *mosmo* forward, 5′—TCTGGATGTTTGTTTCTGGCTGC—3′, *mosmo* reverse, 5′—GGGTAATTTGTAGGGTTGGCCTC—3′, *uqcrc2* forward, 5′—TCCTCTCTAGGAGGCTTTACTCTG—3′, *uqcrc2* reverse, 5′—GGGAGCCAATTTCACCAATCAG—3′, *cdr2* forward,

5′—GACAGCAACGTGGAGGAGTTC—3′, and *cdr2* reverse, 5′—GCGCAGATCATACAGCTCCTTC—3′. The antisense digoxigenin-labeled hybridization probes were transcribed *in vitro* using the T7 MAXIscript kit. Embryos were imaged using a Zeiss AxioCam MRc attached to a Zeiss SteREO Discovery. V8 light microscope. Images were processed in ImageJ.

Cartilage Staining

At stage 42, *Xenopus* embryos were anesthetized with benzocaine and fixed in 4% paraformaldehyde in PBS overnight. Alcian blue staining of embryos was performed based on the Harland Lab protocol. Before ethanol dehydration, embryos were bleached under a fluorescent light in 1.8x saline-sodium citrate, 1.5 H_2O_2, and 5% (vol/vol) formamide for 30 min. Embryos were imaged in PBS, using a Zeiss AxioCam MRc attached to a Zeiss SteREO Discovery V8 light microscope. Images were processed in ImageJ. Analysis of cartilage structures was performed in ImageJ utilizing the polygon, area, and line functions. Measurements included the average ceratohyal area (outlined cartilage in **Figure 2**), and the branchial arch width, which was quantified by taking the width of the branchial arch across the widest point. Differences were analyzed by student's unpaired *t*-test using Graphpad (Prism).

Half-Embryo Injections

Half KDs were performed at the two-cell stage. *X. laevis* embryos were unilaterally injected two times with either control MO or 16p12.1 gene-specific MO and a *gfp* mRNA construct. The other blastomere was left uninjected. Embryos were raised in 0.1X MMR through neurulation, then sorted based on left/right fluorescence. For NCC specification experiments, embryos were fixed at stage 16, and for pharyngeal arch (PA) visualization, embryos were fixed between stage 25–30. Whole-mount *in situ* hybridization

was then performed according to the previously described procedure. Analysis of NCC specification markers from *in situ* experiments was performed on dorsal view images in ImageJ by measuring the total area of expression using the polygon tool. Analysis of PAs from *in situ* experiments was performed on lateral view images in ImageJ. Measurements were taken to acquire: 1) arch area, the area of individual PA determined using the polygon tool, 2) arch length, the length of the distance between the top and bottom of each PA, and 3) arch migration, the ventral most part of the PA to the neural tube. All measurements were quantified by taking the ratio between the injected side versus the uninjected side for each sample, respectively. Statistical significance was determined using a student's unpaired *t*-test in Graphpad (Prism).

Neural Crest Explants, Imaging, and Analysis

Embryos at stage 17 were placed in modified DFA solution (53 mM NaCl, 11.7 mM NA_2CO_3, 4.25 mM K Gluc, 2 mM MgSO4, 1 mM $CaCl_2$, 17.5 mM Bicine, with 50 ug/mL Gentamycin Sulfate, pH 8.3), before being stripped of vitelline membranes and imbedded in clay with the anterior dorsal regions exposed. Skin was removed above the NCC using an eyelash knife, and NCCs were excised. Explants were rinsed, and plated on fibronectin-coated coverslips in imaging chambers filled with fresh DFA. Tissues were allowed to adhere for forty-five minutes before being moved to the microscope for time-lapse imaging of NCC motility. Microscopy was performed on a Zeiss Axio Observer inverted motorized microscope with a Zeiss 20x N-Achroplan 0.45 NA Phase-contrast lens, using a Zeiss AxioCam camera controlled with Zen software. Images were collected using large tiled acquisitions to capture the entire migratory field. Eight to ten explants, from both control and experimental conditions, were imaged at a six-minute interval, for 6 hours. Data was imported to ImageJ, background subtracted, and cropped to a uniform field size. Migration tracks of individual cells were collected manually using the Manual Tracking plug-in. Mean speed rates were imported to Graphpad (Prism), and compared between conditions using student's unpaired t-tests. Three independent experiments were performed for each condition.

For NCC proliferation, NCC tissue explants were allowed to adhere and migrate on fibronectin-coated coverslips for 4 hours before being fixed in 4% paraformaldehyde in PBS. Explants were permeabilized in 0.1% Triton-X 100 in PBS, blocked with a solution containing 2% bovine serum albumin, 0.1% Triton-X 100 in PBS, and incubated in Phospho-Histone H3 (Ser10) (Invitrogen, PA5-17869, polyclonal, 1:500), goat anti-rabbit Alexa $Fluor^{488}$ conjugate secondary antibody (Invitrogen, 1:1000), Alexa $Fluor^{568}$ phalloidin (Invitrogen, 1:500), and Hoechst 33342 solution (Invitrogen, 1:1000). Microscopy was performed on a Zeiss AiryScan inverted motorized microscope with a Zeiss 20X lens, using a Zeiss AxioCam camera controlled with Zen software. Images were acquired using large tiled acquisitions to capture the entire migratory field. Images of five to seven explants, from both control and experimental conditions were imported to ImageJ, and the total number of PH3-labeled positive cells versus the total number of cells were quantified using an automated particle counter after thresholding each image. Cell counts were imported to Graphpad (Prism), and compared between conditions using student's unpaired *t*-test. Three independent experiments were performed for each condition.

RESULTS

16p12.1-Affected Genes Display Expression in the Developing Nervous System, Pharyngeal Arches, and Craniofacial Structures

One of the more prominent symptoms in patients with the 16p12.1 deletion are craniofacial dysmorphisms with varying severity (Girirajan et al., 2010). Children often present with facial asymmetries, micrognathia, a short philtrum, small and deep-set eyes, hypertelorism, a depressed nasal bridge, and dysplastic ears. Comorbidities commonly include microcephaly, growth retardation, scoliosis, and defects in hand and foot development (Girirajan et al., 2010). As proper NCC specification, proliferation, and migration are critical for governing embryonic facial patterning (Gross and Hanken, 2008; Kerney et al., 2012), we hypothesized that one or more of the 16p12.1-affected genes are required for NCC development, and that their depletion would result in defects associated with one or more of these NCC-related processes.

First, we investigated the spatiotemporal expression of four 16p12.1-affected gene orthologs, *polr3e*, *mosmo*, *uqcrc2*, and *cdr2*, across multiple stages of development in *Xenopus laevis* embryos. To examine this, we performed whole-mount *in situ* hybridization with DIG-labeled antisense RNA probes against these four genes (**Figure 1**; **Supplementary Figure S3**; for *in situ* hybridization controls against RNA sense strands, see **Supplementary Figure S4**). Interestingly, we observed primarily ubiquitous expression of all four gene transcripts during early blastula and gastrula stages (st. 10 and 13; data not shown; st. 20; **Supplementary Figures S3A,B, E,F, I,J, M,N**), although there were some gene-specific differences apparent by stage 20. For example, there appeared to be a small enrichment in *polr3e* in putative neural crest at the borders of the neural plate, as well as an enrichment of *uqcrc2* in the anterior embryo. However, by stage 25, more defined expression became visible during early craniofacial morphogenesis, with expression of each gene in migratory NCCs that reside in the pharyngeal arches (**Figures 1B–E**). The expression patterns of *polr3e* and *mosmo* are similar to the NCC-enriched transcription factor, *twist* (**Figure 1A**). At this stage, expression of both *polr3e* and *mosmo* is particularly strong in the developing brain and eye, which is consistent with previous data suggesting that these genes are important for both brain and eye development (Pizzo et al., 2021). The expression patterns of *uqcrc2* and *cdr2* appear to be more restricted to the

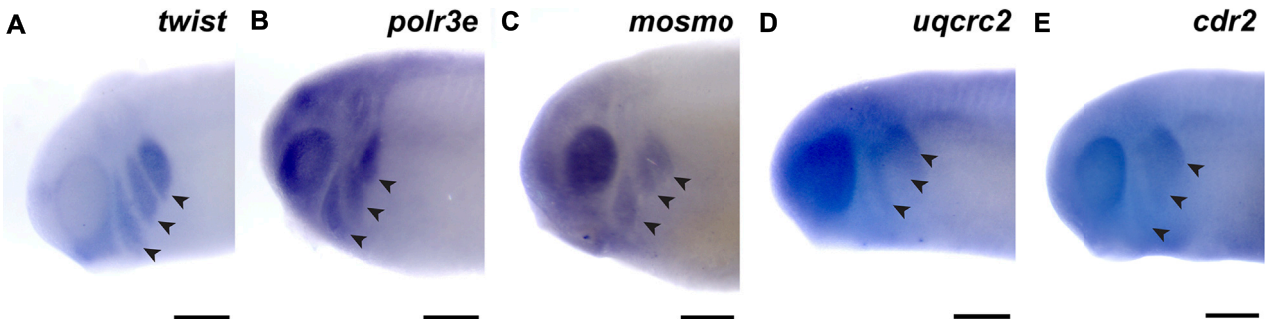

FIGURE 1 | 16p12.1-affected genes are expressed in migrating neural crest cells during embryonic development. **(A)** Lateral view of whole-mount *in situ* hybridization at stage 25 for *twist*, a NCC-enriched transcription factor. Anterior of embryo is to left. Arrows indicate the pharyngeal arches (PAs). **(B–E)** *In situ* hybridization at stage 25–28 for *polr3e*, *mosmo*, *uqcrc2*, and *cdr2* demonstrate expression in NCCs that occupy the PAs (n = 10 per probe). Scalebar = 300 μm.

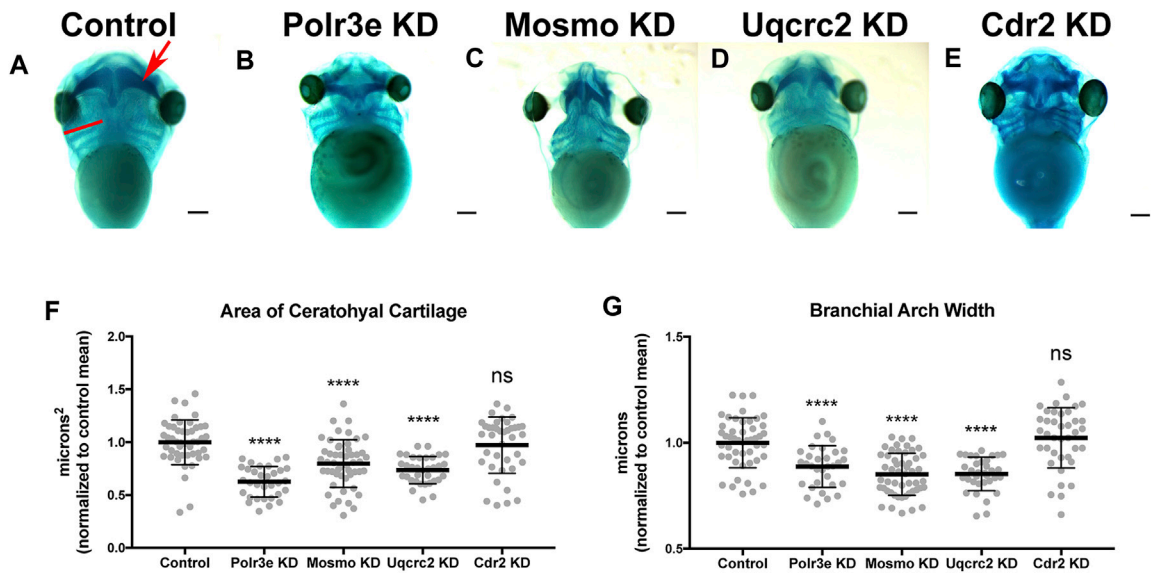

FIGURE 2 | Knockdown of Polr3e, Mosmo, and Uqcrc2 impact cartilage morphology. **(A–E)** Ventral view of stage 42 embryos following single 16p12.1-associated gene KD, stained with Alcian blue to label cartilage elements. Anterior of embryo is at the top. In the control, the red arrow points to ceratohyal cartilage, while the red bar spans the first branchial arch. **(F–G)** Measurements of the average ceratohyal area and width of the first branchial arch. The data was normalized to the control MO condition. Partial depletion of Polr3e, Mosmo, and Uqcrc2 significantly reduced the size of both of these cartilage elements compared to controls, while depletion of Cdr2 had no effect on cartilage size. Significance determined using a student's unpaired *t*-test. (Embryos quantified: Control = 48, Polr3e KD = 32, Mosmo KD = 51, Uqcrc2 KD = 34, Cdr2 KD = 39). ****$p < 0.0001$, ***$p < 0.001$, **$p < 0.01$, *$p < 0.05$, n.s., not significant. Scalebar = 300 μm.

posterior of the NCC migration stream. All four genes are expressed in the developing head and facial structures throughout stage 35 (**Supplementary Figures S3C,D, G,H, K,L, O,P**), although they each display distinct patterns throughout these tissues. *Polr3e* expression is strong in most of the pharyngeal arches and also becomes more defined in the hindbrain region, whereas *mosmo* expression is stronger in the forebrain region (**Supplementary Figures S3C,G**). *Uqcrc2* has specific expression in hyoid and branchial arches compared to the mandibular, with diffuse staining throughout the face, and there is also expression in the developing kidney and somites (**Supplementary Figure S3K**). By stage 40, *mosmo* expression is also observed in the developing spinal cord (**Supplementary Figure S3H**). Additionally, the expression patterns of all four genes show potential overlap with cardiac tissue (**Supplementary Figures S3D,H,L,P**). Thus, our findings demonstrate that the four 16p12.1-gene orthologs display expression in the developing nervous system, migratory NCCs in the pharyngeal arches, and later craniofacial structures, among other tissues.

Several 16p12.1-Affected Genes Are Important for Maintaining Cartilage Size and Scaling

Many individuals with the 16p12.1 deletion display defects in cartilage and skeletal development including deformed nose and

ears, tooth malformation, short stature, smaller head size, and delayed growth (Girirajan et al., 2010). Additionally, patients also have speech, feeding, and swallowing impairments that are linked to abnormal jaw and throat formation (Girirajan et al., 2010). As these cartilaginous and skeletal tissues are derived from NCCs (Etchevers et al., 2019; Merkuri and Fish, 2019; Szabo and Mayor, 2018; Van Otterloo et al., 2016), we hypothesized that one or more of the 16p12.1-affected genes may play an essential role during embryonic development of craniofacial cartilage and skeletal structures. To examine this, we performed partial depletion of the four 16p12.1 gene orthologs to determine their influence on cartilage scaling in *Xenopus laevis* embryos (**Figure 2**). As the human disorder is due to a hemizygous deletion, we sought to achieve 50% knockdown in an attempt to recapitulate the gene dosage of the human condition. Thus, we utilized morpholino antisense oligonucleotides, which we previously validated to achieve 50% knockdown for each gene (**Supplementary Figures S1, 2**) (Pizzo et al., 2021).

Reduced dosage of *polr3e*, *mosmo*, and *uqcrc2* was sufficient to severely impact cartilage development of stage 42 embryos. When we knocked down these three genes individually (throughout the entire embryo), we observed overt defects on cartilage morphology compared to controls (**Figures 2B–D**), including a decrease in the average ceratohyal area and the width of the first branchial arch (**Figures 2F,G**). Surprisingly, given that we previously showed that partial depletion of *cdr2* led to a minor reduction in facial size (Pizzo et al., 2021), it did not result in similar overt cartilage abnormalities (**Figure 2E**), nor was there any obvious effect on the size of individual cartilage elements (**Figures 2F,G**). However, reduced dosage of *cdr2* does still lead to a morphological change in the ceratohyal shape which, while not quantified in our assay, still might have a significant functional impact if the same change were found in human patients. It is also possible that there may be genetic compensation by other closely related genes such as *cdr1*, *cdr2-like*, and *cdr3*. Overall, these results indicate that Polr3e, Mosmo, and Uqcrc2 are essential for early cartilaginous tissue formation and are likely important for later development of head and facial skeletal structures. Moreover, these results demonstrate that partial depletion of the 16p12.1-associated genes creates persistent defects on craniofacial patterning and cartilage formation that are not ameliorated later in development (stage 42), leading to our hypothesis that these genes may impact processes important for the embryonic progenitors of these tissues.

Several 16p12.1-Affected Genes are Critical for Normal Pharyngeal Arch Migration and NCC Motility

Given that the 16p12.1-affected gene transcripts display expression in NCCs residing in the pharyngeal arches during stages that correspond with their migration (st. 25-30), we hypothesized that depletion of one or more of these genes may disrupt NCC migration and motility. To test this, we utilized single-blastomere injection strategies to generate left-right chimeric embryos, allowing for a side-by-side comparison of *twist* expression patterns between wild-type or KD sides, and we tracked the progress of migratory NCCs (**Figure 3**). Following single-sided individual depletion of each 16p12.1 gene, embryos were staged to 25-28, fixed, and *in situ* hybridization was performed against *twist*. To quantify NCC migration away from the anterior neural tube, measurements were taken of the total pharyngeal arch (PA) area, length of each individual pharyngeal arch (designated "arch length" in **Figure 3**) (**Supplementary Figure S5**), and total migration distance of the NCCs that form each individual pharyngeal arch (designated "arch migration"), for both the uninjected and control or KD side of each embryo (**Figures 3F–Q**). We found that Polr3e and Mosmo knockdown significantly reduced total area of NCC streams (**Figures 3F,G**). Further, when Polr3e levels were reduced, the posterior PA was shorter in length (**Figure 3J**), whereas knockdown of Mosmo reduced the length of the anterior PA and hyoid PA (**Figure 3L**). Additionally, individual depletion of these genes reduced the ventral migration distance of all three NCC streams compared to controls (**Figures 3K,M**). Interestingly, knockdown of Uqcrc2 resulted in an increase in total PA area (**Figure 3H**) and a slight increase in the length of the anterior and hyoid PAs (**Figure 3N**), though it did not impact NCC migration (**Figure 3O**). It is possible that NCC proliferation is upregulated to compensate for reduced Uqcrc2 levels, leading to an increase in PA area and length. While knockdown of Cdr2 slightly increased hyoid PA length (**Figure 3P**), it did not result in significant changes in PA area or NCC migration (**Figures 3I,Q**). Together, these results suggest a specific role for Polr3e, Mosmo, and Uqcrc2 in maintaining NCC migration *in vivo*.

While the previous experiment suggested a possible role for Polr3e, Mosmo, and Uqcrc2 in regulating NCC migration, other NCC-related defects might also lead to changes in measured PA area, length, and NCC migration distance. Thus, to investigate whether reduced dosage of any of the 16p12.1-affected genes impacted NCC migration rate itself, *in vitro* migration assays were performed, as previously described (Lasser et al., 2019; Mills et al., 2019). Individual genes were partially depleted in the whole embryo and NCCs were dissected prior to delamination from the neural tube (st. 17) from both KD and control conditions. These tissue explants were cultured on fibronectin-coated coverslips and individual cell migration for each explant was imaged using time-lapse phase-contrast microscopy for 6 hours (**Figures 4A–E, A′–E′**). Trajectories and speed of individual cells that escaped the explant were then mapped using automated particle tracking (**Figure 4F**) (Schindelin et al., 2012; Tinevez et al., 2017). Partial knockdown of Polr3e and Uqcrc2 resulted in slower individual NCC speed compared to controls (**Figures 4G,I**), while partial knockdown of Mosmo did not significantly impact NCC speed (**Figure 4H**). Thus, we show that knockdown of Polr3e and Uqcrc2 alters NCC migration into the PAs, and that this defect could be driven by a reduction in individual NCC motility rates.

As partial knockdown of Cdr2 was not sufficient to significantly alter NCC streaming *in vivo*, nor was it sufficient to cause severe craniofacial or cartilage morphology defects, we hypothesized that NCC motility *in vitro* would not be affected by this depletion. Instead, knockdown of Cdr2 led to a significant increase in the speed of CNCs migrating *in vitro* (**Figure 4J**). One possibility that

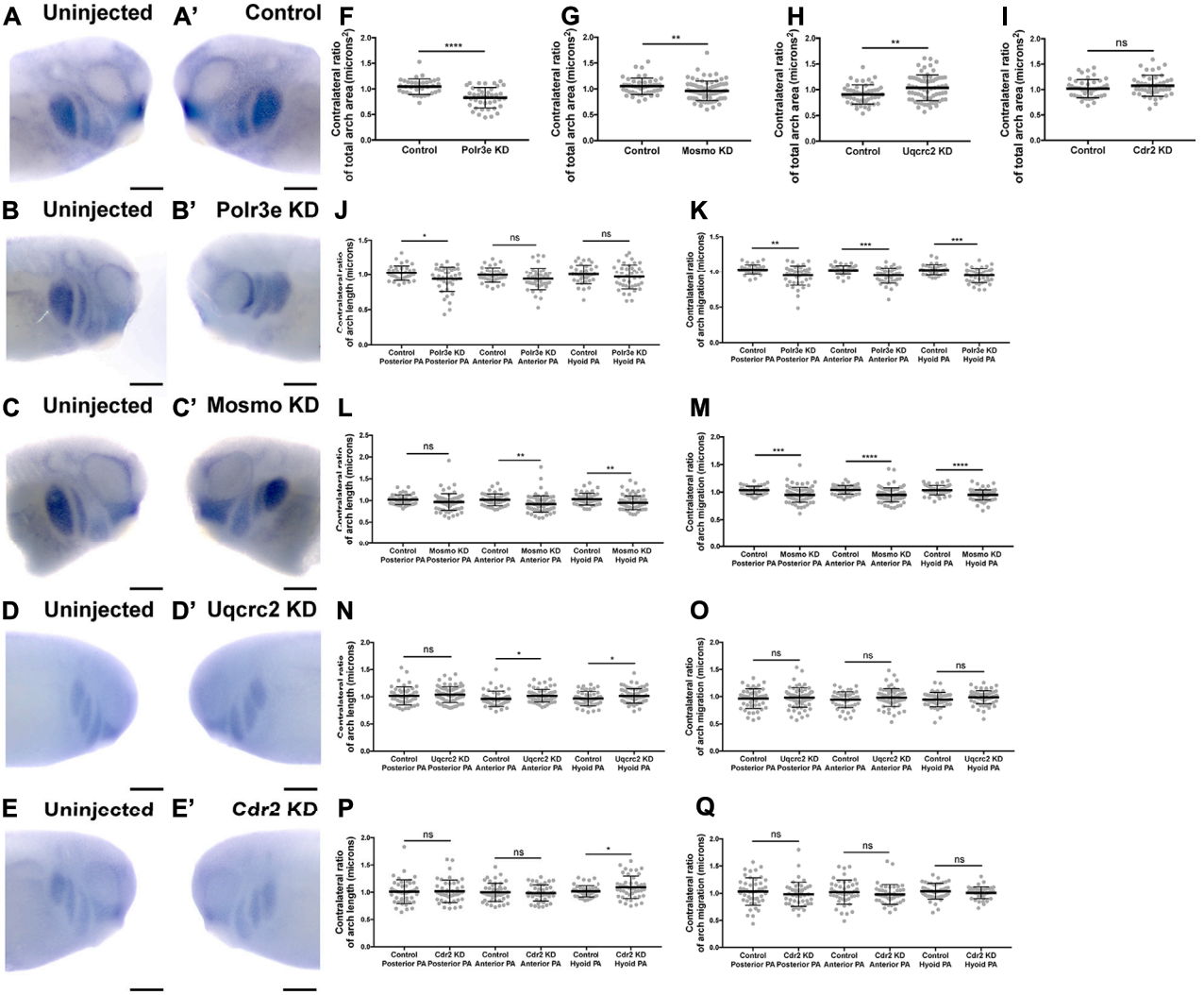

FIGURE 3 | Knockdown of Polr3e and Mosmo affect CNC migration *in vivo*. **(A–C, A′–C) (A–E, A′–E′)** Lateral views of stage 25 embryos following whole-mount *in situ* hybridization against *twist*. Each column of panels are lateral views of two sides of the same embryo. Embryos were unilaterally injected to KD each individual 16p12.1-affected gene in half of the embryo and the other half was left uninjected. The left panels **(A–E)** represent the uninjected side and the right panels **(A′–E′)** represent the injected side. **(F–Q)** Measurements were taken for the total area of the three PAs (posterior PA, anterior PA, and hyoid PA), the length of each individual arch, and the NCC migration distance, as measured from the dorsal-most tip of each arch to the neural tube, by taking ratios of the injected side versus the uninjected side. Significance was determined using an unpaired students *t*-test with these ratios. **(F–H)** Partial depletion of both Polr3e and Mosmo significantly reduced the total area of the three PAs, while partial depletion of Uqcrc2 slightly increased the total area of the three PAs. **(J–K)** Polr3e KD significantly reduced the length of the posterior PA but had no effect on the length of the anterior PA or hyoid PA. However, partial depletion of this gene significantly reduced the total NCC migration distances for all three PAs. **(L–M)** Mosmo KD significantly reduced the length of the anterior PA and hyoid PA but had no effect on the length of the posterior PA. Partial depletion of this gene also significantly reduced the total NCC migration distance for all three PAs. **(N–O)** Uqcrc2 KD slightly increased the length of the anterior and hyoid PA but had no effect on the length of the posterior PA, nor did it affect the total NCC migration distance. **(I, P–Q)** Cdr2 KD had no effect on the total area of the three PAs, nor did it affect the total NCC migration distance. However, partial depletion of this gene slightly increased the length of the hyoid PA but did not affect the posterior or anterior PAs. (Embryos quantified: Control for Polr3e = 35, Control for Mosmo = 48, Control for Uqcrc2 = 48, Control for Cdr2 = 45, Polr3e KD = 41, Mosmo KD = 75, Uqcrc2 KD = 68, Cdr2 KD = 45). ****$p < 0.0001$, ***$p < 0.001$, **$p < 0.01$, *$p < 0.05$, n.s., not significant. Scalebar = 300 μm.

individual cell speed of Cdr2 KD *in vitro* does not directly correspond to differences in NCC streaming *in vivo* is that the boundaries of NCC migration *in vivo* are heavily restricted due to repellent guidance cues within the PAs. However, there could be other reasons, for example, as expression of *cdr2* occurs more in the posterior NCC stream and possibly mesoderm, *cdr2* might not be utilized cell autonomously in NCC development.

16p12.1-Affected Genes do Not Directly Impact NCC Proliferation in Explants

As NCCs exit the dorsal neural tube and undergo directed migration along stereotypical pathways during vertebrate development, they must also balance between cell division and migration (Szabo and Mayor, 2018). Reduced gene dosage

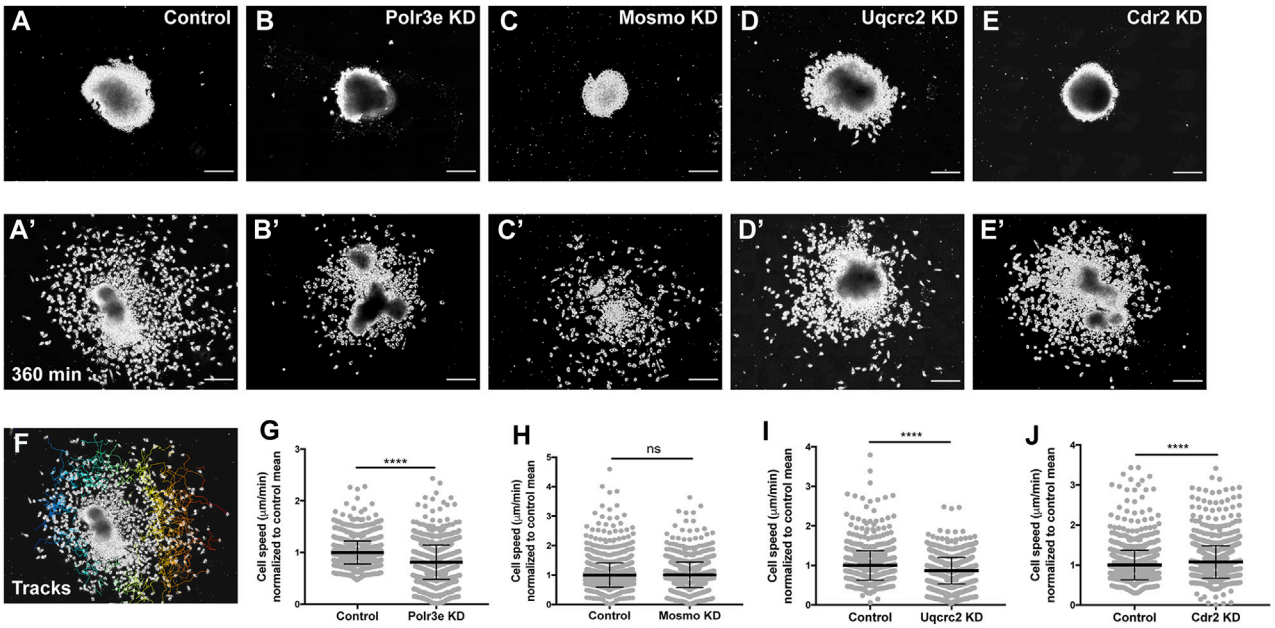

FIGURE 4 | Manipulation of Polr3e, Uqcrc2, and Cdr2 impacts NCC migration speeds *in vitro*. Dissected NCC explants from control, Polr3e KD, Mosmo KD, Uqcrc2 KD, or Cdr2 KD embryos were plated on fibronectin-coated coverslips, allowed to adhere and begin migration, and imaged for 6 h using 20x phase microscopy. **(A–E)** Representative images of explants at initial timepoint (0 min). **(A′–E′)** Representative images of explants after 6 h migration (360 min). **(F)** Representative tracks generated by FiJi Trackmate plug-in overlaid on panel A'. **(G–J)** Mean track speeds of Polr3e KD, Mosmo KD, Uqcrc2 KD, and Cdr2 KD explants compared to their controls. Partial depletion of Polr3e and Uqcrc2 significantly reduced mean NCC speed, while depletion of Cdr2 increased mean NCC speed. Partial depletion of Mosmo had no effect on mean NCC speed. (Explants quantified: 6-7 explants from control and KD embryos were plated for each experiment. Three separate experiments were performed for each depletion.) $^{****}p < 0.0001$, $^{***}p < 0.001$, $^{**}p < 0.01$, $^{*}p < 0.05$, n.s., not significant. Scalebar = 200 μm.

could result in smaller areas of *twist* expression due to decreased cellular migration rates, but it is also possible that there are fewer NCCs within the PAs if genetic manipulations affect NCC proliferation rates. To address this, each 16p12.1 gene was individually depleted in the whole embryo and NCCs were dissected as described in the previous section. These tissue explants were cultured on fibronectin-coated coverslips and NCCs were allowed to migrate away from the explant for 4 hours before being fixed. Immunocytochemistry was then performed using a phospho-histone H3 (PH3) antibody as a marker for cell proliferation (**Figures 5A–A'**). To measure NCC proliferation, the number of cells positively labeled for PH3 versus the total number of cells per explant were quantified using an automated particle counter after thresholding each image. We found that partial depletion of individual 16p12.1-affected genes had no statistically significant effect on NCC proliferation *in vitro* (**Figures 5B–E**). Division of NCCs occurs over a wide range of times after exiting the neural tube, with mitotic activity significantly increasing as cells enter the pharyngeal arches (Gonsalvez et al., 2015; Rajan et al., 2018). Thus, it is possible that we do not observe a direct effect on NCC proliferation due to the absence of *in vivo* microenvironmental signals that are necessary for cell division.

Several 16p12.1-Affected Genes are Critical for NCC Induction and Specification

The process of NCC induction and specification is complex and requires a specific level of signaling by the BMP, Wnt, FGF, RA, Shh, and Notch/Delta pathways to establish a gene regulatory network that is crucial for determining NCC identity (Villanueva et al., 2002; Monsoro-Burq et al., 2003; Wu et al., 2005; Theveneau and Mayor, 2012; Pla and Monsoro-Burq, 2018; Rogers and Nie, 2018; Prasad et al., 2019). During the early steps of NCC formation, these morphogen pathways work in concert with various NCC transcription factors (TFs) such as *snai1*, *snai2/slug*, *sox9*, and *twist*, to establish the neural plate border, regulate NCC specification, and subsequent NCC migration (Aybar et al., 2003; del Barrio and Nieto, 2002; LaBonne and Bronner-Fraser, 1998, 2000; Pla and Monsoro-Burq, 2018; Rogers and Nie, 2018; Spokony et al., 2002). As shown in the previous sections, we found that partial depletion of several 16p12.1-affected genes significantly impacted *twist* expression patterns and NCC migration in the PAs, and that these defects were not due to changes in NCC proliferation rates. However, it is possible that reduced dosage of these genes causes NCC migration defects due to changes in NCC specification, resulting in fewer numbers of cells. Therefore, we tested this by utilizing single-blastomere injection strategies to generate left-right chimeric embryos, and compared side-by-side

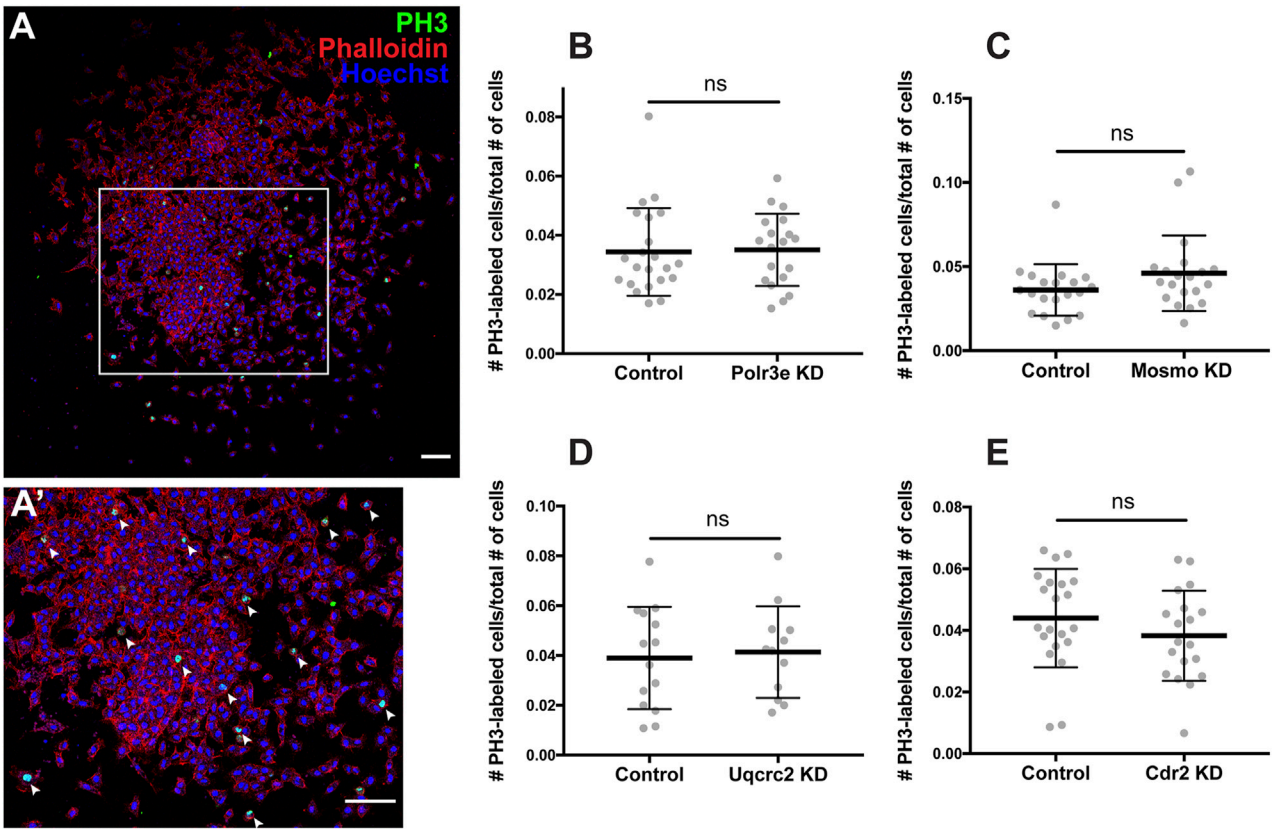

FIGURE 5 | Manipulation of 16p12.1-affected genes does not impact NCC proliferation *in vitro*. Dissected NCC explants from control, Polr3e KD, Mosmo KD, Uqcrc2 KD, and Cdr2 KD embryos were plated on fibronectin-coated coverslips, allowed to adhere and begin migration for 4 h before being fixed in 4% PFA and immunostained with PH3 antibody as a marker for NCC proliferation, phalloidin to label the actin cytoskeleton, and Hoechst to label nuclei. **(A,A')** Representative image of control NCC explant immunostained with PH3, phalloidin, and Hoechst. White arrows denote cells positively labeled for PH3. **(B–E)** Quantification of the number of positively PH3-labeled cells versus the total number of cells per NCC explant for Polr3e KD, Mosmo KD, Uqcrc2 KD, and Cdr2 KD compared to controls. Partial depletion of each individual 16p12.1-affected did not have a significant impact on NCC proliferation *in vitro*. (Explants quantified: 6-7 explants from control and KD embryos were plated for each experiment. Three separate experiments were performed for each depletion). $^{****}p < 0.0001$, $^{***}p < 0.001$, $^{**}p < 0.01$, $^{*}p < 0.05$, n.s., not significant. Scalebar = 300 μm.

expression patterns of TFs required for NCC induction and specification between wild-type and KD sides.

Following single-sided individual depletion of each 16p12.1 gene, embryos were f ixed at st. 16 and *in situ* hybridization was performed against *sox9* or *twist* (**Figures 6A–J**). To quantify changes in expression of NCC specification markers, measurements were taken of the total area of expression of each marker for both the uninjected and control or KD side of each embryo (**Figures 6A–J**). Although both NCC specification markers were present, there were clear abnormalities including reduced signal and smaller total area of expression following partial knockdown of either Polr3e or Mosmo (**Figures 6C–F,K–L**). In contrast, knockdown of Uqcrc2 or Cdr2 did not significantly affect the signal or total area of expression for either NCC specification marker (**Figures 6G–L**). Together, these results suggest that Polr3e and Mosmo are distinctly required for NCC specification, as reduced levels alter expression of NCC specification markers, which may result in fewer cells and subsequent PA defects.

DISCUSSION

To functionally explore the basis of the craniofacial and cartilage defects associated with the 16p12.1 deletion, we analyzed craniofacial phenotypes and cellular mechanisms underlying decreased dosage of four genes affected within this region. Our results show that three genes impacted by this CNV can contribute to normal craniofacial morphogenesis in *Xenopus laevis* (**Figure 7**), in a model where decreased gene dosage leads to both global and specific effects. We also provide evidence that deficits during NCC development may contribute to the craniofacial dysmorphisms associated with the deletion. Specifically, we demonstrate, for the first time, that the 16p12.1-affected genes are co-expressed in motile NCCs and contribute to normal craniofacial patterning and cartilage formation. Several of these genes also directly impact NCC migration *in vivo* (*polr3e, mosmo*, and *uqcrc2*), NCC motility (*polr3e* and *uqcrc2*), and NCC specification (*polr3e* and *mosmo*), revealing new basic roles for these genes during embryonic development.

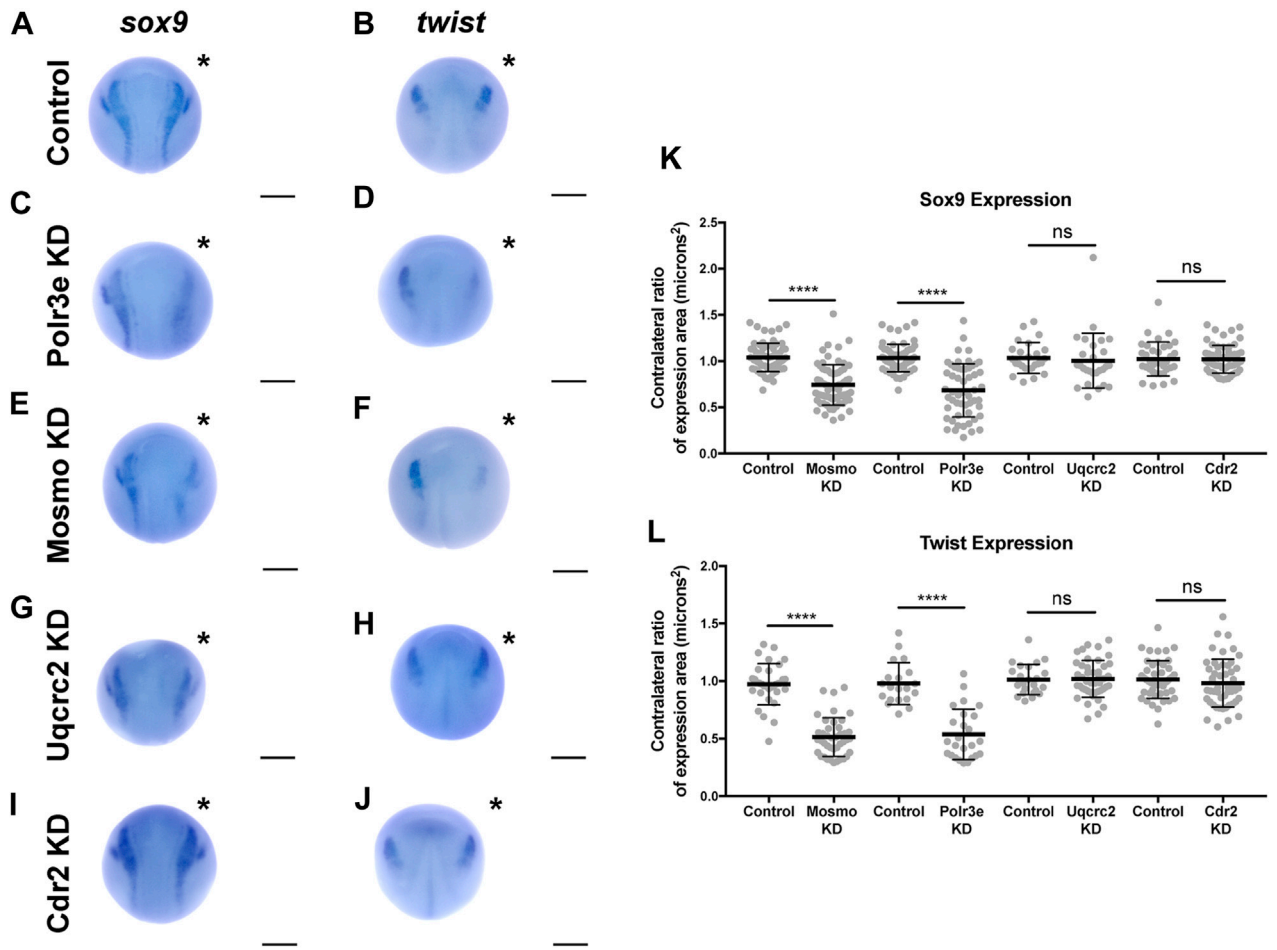

FIGURE 6 | Manipulation of Polr3e and Mosmo affects NCC specification *In situ* hybridization utilized **(A,C,E,G,I)** antisense mRNA probe against *sox9* and **(B,D,F,H,J)** antisense mRNA probe against *twist*. Each column of panels are dorsal views of two sides of the same embryo. Embryos were unilaterally injected to KD each individual 16p12.1-affected gene in half of the embryo and the other half was left uninjected. The left side represents the uninjected side and the right side, indicated with an asterisk (*), represents the injected side. Anterior of embryo is at the top. **(K–L)** Measurements were taken for the total area of the expression pattern for either *sox9* **(K)** or *twist* **(L)** using the polygon tool in ImageJ by taking ratios of the injected side versus the uninjected side. Significance was determined using an unpaired students *t*-test with these ratios. Partial depletion of either Mosmo or Polr3e significantly reduced the total area of expression for both *sox9* and *twist*, while partial depletion of either Uqcrc2 or Cdr2 did not significantly affect the total area of expression for either NCC specification marker. (Embryos quantified with *sox9* probe: Control for Polr3e = 60, Control for Mosmo = 66, Control for Uqcrc2 = 25, Control for Cdr2 = 36, Polr3e KD = 55, Mosmo KD = 69, Uqcrc2 KD = 27, Cdr2 KD = 59. Embryos quantified with *twist* probe: Control for Polr3e = 20, Control for Mosmo = 33, Control for Uqcrc2 = 23, Control for Cdr2 = 46, Polr3e KD = 25, Mosmo KD = 41, Uqcrc2 KD = 44, Cdr2 KD = 50). ****$p < 0.0001$, ***$p < 0.001$, **$p < 0.01$, *$p < 0.05$, n.s., not significant. Scalebar = 300 μm.

As the 16p12.1 deletion is multigenic in nature, we sought to determine each gene's contribution to a craniofacial phenotype. Although we have narrowed our studies to focus on how each individual 16p12.1-affected gene contributes to facial patterning, our findings align with the idea that the presentation of symptoms associated with the deletion is a cumulative product of the impacted region. While *polr3e* and *mosmo* knockdowns severely impacted nearly all examined aspects of craniofacial morphogenesis and NCC development across early developmental stages, *uqcrc2* and *cdr2* knockdowns produced very minimal or no phenotypes in these areas.

In particular, we observed a global functional role for *polr3e*, *mosmo*, and *uqcrc2* in both craniofacial and cartilage development. Individual depletion of these genes narrowed facial width and area, and decreased eye size in a way that appears analogous to the smaller head and smaller eye size phenotypes observed in children with the 16p12.1 deletion (Pizzo et al., 2021). Moreover, reduced levels of these genes decreased the size of cartilaginous tissue structures important for jaw and mouth formation, which may correlate with the micrognathia phenotype. However, the phenotypes associated with *uqcrc2* KD were quite mild in comparison to *polr3e* or *mosmo* KD, and *cdr2* KD had little to no effect on craniofacial or cartilage formation. Thus, further investigation into how these gene depletions function combinatorially to generate the full signature of the 16p12.1 deletion craniofacial dysmorphism is necessary.

16p12.1 gene	Craniofacial Morph.	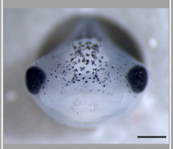	Cartilage Morph.	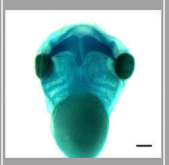	PA migration	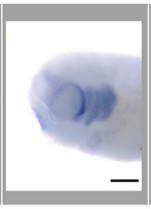	NCC motility	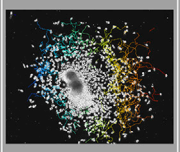	NCC proliferation	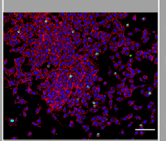	NCC specification	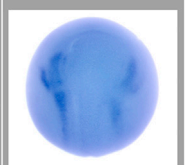
Mosmo	✓	Reduced Size of facial features	✓	Reduced Size of cartilage elements	✓	Reduced Arch area, length, migration	✗	No phenotype	✗	No phenotype	✓	Reduced Expression of *sox9* and *twist*
Polr3e	✓	Reduced Size of facial features	✓	Reduced Size of cartilage elements	✓	Reduced Arch area, length, migration	✓	Reduced Mean NCC speed	✗	No phenotype		Reduced Expression of *sox9* and *twist*
Uqcrc2	✓	Reduced Size of facial features	✓	Reduced Size of cartilage elements	✓	Increased Arch area, length	✓	Reduced Mean NCC speed	✗	No phenotype	✗	No phenotype
Cdr2	✓	Reduced Size of facial features	✗	No phenotype	✓	Increased Arch length	✓	Increased Mean NCC speed	✗	No phenotype	✗	No phenotype

FIGURE 7 | Summary table of 16p12.1-affected gene craniofacial, cartilage, and NCC phenotypes. Partial depletion of 16p12.1-affected genes demonstrates numerous impacts on craniofacial, cartilage, and CNC development. Tissues are denoted as affected (checked box) if phenotypes were significantly different from control ($p < 0.05$); see individual figures for data distribution and statistics.

It should be mentioned that depletion of the 16p12.1-affected genes in *X. laevis* almost certainly diverges from perfect recapitulation of the 16p12.1 deletion symptoms. *Xenopus* has emerged as a powerful model system to study human genetic diseases of craniofacial development, as the majority of disease-associated pathways that drive craniofacial morphogenesis are conserved between these species (Tahir et al., 2014; Dickinson, 2016; Dubey and Saint-Jeannet, 2017; Devotta et al., 2018; Griffin et al., 2018; Lasser et al., 2019; Mills et al., 2019; Lichtig et al., 2020; Schwenty-Lara et al., 2020). However, not only does the CNV contain non-coding regions that we did not model here, but there are also some craniofacial and cartilage morphological differences between *Xenopus* and humans that prevent certain direct correlations to disease pathology. For example, NCCs residing in the hyoid PA, that give rise to the ceratohyal cartilage in *Xenopus,* will later give rise to anterior portions of the face and combine with contributions from the Meckel's cartilage to form regions of the lower jaw (Gross and Hanken, 2008; Kerney et al., 2012). In humans, Meckel's cartilage will similarly form portions of the lower jaw but will also become part of the middle ear skeletal structures. Therefore, morphological impacts resulting from aberrant development of these tissues may have more direct correlates to human pathology in the context of NCC migration and development of the PAs.

Within that effort, our work has demonstrated co-expression of these gene transcripts in NCCs and their necessity during specific NCC-related processes which may be a driving mechanism underlying the observed craniofacial and cartilage defects. Decreased dosage of *polr3e* or *mosmo* significantly affected PA migration *in vivo* leading to decreased PA area, length, and NCC migration distance from the neural tube. Although *uqcrc2* KD led to both craniofacial and cartilage defects, surprisingly, its depletion caused an increase in PA area and length. Our data suggests that these PA migration defects may be due to gene-specific effects during aspects of NCC development, as *polr3e* KD impacted both NCC motility and specification, *mosmo* KD impacted NCC specification, and *uqcrc2* KD impacted NCC motility.

While we show that several 16p12.1-affected genes are important for regulating NCC development and subsequent formation of their tissue derivatives, it remains unclear as to why any of these genes may be exceptionally critical in these tissues. Given that they are all generally expressed in the pharyngeal arches and NCC regions, it might be somewhat surprising that only two were associated with major effects. This could be due to compensation from other closely related genes for *uqcrc2* and *cdr2* (the two genes that did not have major NCC defects), or it could also be that, within the 16p12.1 region, *polr3e* and *mosmo* are more sensitive to fluctuations of dosage levels than *uqcrc2* and *cdr2*. We also note that there were no other obvious abnormalities in the embryos beyond the craniofacial and brain phenotypes that we report. However, we have not specifically tested other tissue and organ systems such as cardiac or GI, and some children with 16p12.1 deletion do also have cardiac and GI symptoms. Thus, it would be worth examining these systems in the future.

One question is how our findings fit within the known roles of these genes, and how they may mechanistically influence NCC-

related processes. POLR3E is a subunit of RNA polymerase III, important for regulating the transcription of small RNAs, such as 5S rRNA and tRNAs (Hu et al., 2002). In our study, depletion of *polr3e* significantly affected NCC specification, suggesting that it may be important for regulating transcription of genes necessary in maintaining the identity and subsequent differentiation of NCCs. Studies suggest that loss-of-function of other subunits of RNA polymerase III, POLR1C and POLR1D, are also associated with craniofacial disorders, and specifically with cartilage hypoplasia and cranioskeletal anomalies, due to deficient ribosome biogenesis, increases in cellular death, and deficiencies in NCC migration (Noack Watt et al., 2016). Given that POLR3E has been shown to interact with POLR1C and POLR1D, it is plausible that it may function in a similar capacity.

Recent work in cell culture suggests that MOSMO acts as a negative regulator of Sonic hedgehog signaling (Shh) by degrading the Frizzled class receptor, Smoothened (Pusapati et al., 2018), and our previous work was the first to show that this gene may play a role in vertebrate embryonic craniofacial development (Pizzo et al., 2021). This has recently been confirmed in zebrafish (Camacho-Macorra et al., 2021). The Shh pathway is known to be critical for craniofacial morphogenesis, as upregulation or downregulation of signaling can lead to aberrant NCC patterning, development, and maintenance (Abramyan, 2019; da Costa et al., 2018; Dworkin et al., 2016; Everson et al., 2017; Grieco and Hlusko, 2016; Hammond et al., 2018; Millington et al., 2017; Okuhara et al., 2019; Wang et al., 2019). This aligns well with our results demonstrating that *mosmo* can directly impact NCC specification, highlighting a new cell biological role for this gene.

UQCRC2 is a component of the mitochondrial respiratory chain complex III that is required for its assembly and is important for normal mitochondrial activity to produce ATP (Miyake et al., 2013; Kurosaka et al., 2014; Gaignard et al., 2017; Hammond et al., 2018). Reduced levels of *uqcrc2* produced both craniofacial and cartilage phenotypes, potentially due to decreased NCC motility. This could be especially damaging in the context of multipotent NCCs, as metabolism is increasingly demonstrated to perform a commanding role in determination of cell fate and subsequent motility (Sperber et al., 2015; Mathieu and Ruohola-Baker, 2017; Perestrelo et al., 2018).

CDR2 is an oncogenic protein that is strongly expressed in the cerebellum (Schubert et al., 2014; Hwang et al., 2016; Venkatraman and Opal, 2016). CDR2 is also believed to play multiple roles in the regulation of transcription by regulating the TF c-Myc, which is required for correct temporal and spatial development of NCCs (Bellmeyer et al., 2003; O'Donovan et al., 2010; Okano et al., 1999). *Cdr2* mRNA can be found in almost all cell types, however, its protein expression is limited to Purkinje neurons, some brainstem areas, and spermatogonia (Venkatraman and Opal, 2016). This lack of protein expression could explain why depletion of this gene in *Xenopus* did not produce significant craniofacial or cartilage defects, nor affect NCC developmental processes. It is also possible that other closely related genes, such as *cdr1*, *cdr3*, or *cdr2l*, can functionally compensate for the lack of *cdr2* levels.

Altogether, it is clear that our current knowledge of how these genes ultimately contribute to embryonic craniofacial and cartilage morphogenesis is lacking, and further basic cell biological examination of 16p12.1-affected gene function within a developmental context is necessary for a better mechanistic understanding of the 16p12.1 deletion etiology. Finally, it will also be essential to explore how these genes ultimately synergistically or epistatically regulate the pathology associated with the 16p12.1 deletion. To this aim, our model provides a unique advantage by being a moderate throughput, titratable, and inexpensive system to combinatorially deplete numerous genes simultaneously. For example, our previous work using combinatorial depletion of *polr3e* and *mosmo* showed an enhancement of the brain development phenotype, thus highlighting that the combined impact of loss of function of these genes could have an important effect (Pizzo et al., 2021). Together, our current and ongoing work suggests significant roles for several 16p12.1-affected genes as potent effectors of NCC-derived tissues that regulate specific processes during their development, providing a foundation for the underlying mechanisms contributing to the craniofacial defects associated with the 16p12.1 deletion.

DATA AVAILABILITY STATEMENT

The raw data supporting the conclusions of this article will be made available by the authors, without undue reservation.

ETHICS STATEMENT

The animal study was reviewed and approved by Boston College and Boston University Institutional Animal Care and use Committees.

AUTHOR CONTRIBUTIONS

ML and LL contributed to conception and design of the study. ML, JB, LM, CO'B, SL performed the experiments. ML performed statistical analysis and wrote the first draft of the manuscript. LL edited the manuscript. All authors contributed to manuscript editing, read, and approved the submitted version.

FUNDING

This work was supported by the National Institutes of Health (R01 GM121907, R01 MH109651, R03 DE025824), the American Cancer Society (RSG-16–144-01-CSM), the Ellison Foundation, and National Science Foundation (Grant No. 1626072).

ACKNOWLEDGMENTS

We thank Helen Willsey for reading and comments on the manuscript. We thank members of the Lowery Lab for helpful discussions, suggestions, and editing. We thank Connor Monahan and Sydney Kim for technical assistance. We thank Nancy McGilloway and Todd Gaines for excellent *Xenopus* husbandry. We also thank the National *Xenopus* Resource (RRID:SCR013731) and Xenbase (RRID:SCR-003280) for their support. We thank Bret Judson and the Boston College Imaging Core for infrastructure and support.

SUPPLEMENTARY MATERIAL

The Supplementary Material for this article can be found online at: https://www.frontiersin.org/articles/10.3389/fgene.2022.833083/full#supplementary-material

REFERENCES

Abramyan, J. (2019). Hedgehog Signaling and Embryonic Craniofacial Disorders. *J. Dev. Biol.* 7. doi:10.3390/jdb7020009

Alonso-Gonzalez, A., Rodriguez-Fontenla, C., and Carracedo, A. (2018). De Novo Mutations (DNMs) in Autism Spectrum Disorder (ASD): Pathway and Network Analysis. *Front. Genet.* 9, 406. doi:10.3389/fgene.2018.00406

Antonacci, F., Kidd, J. M., Marques-Bonet, T., Teague, B., Ventura, M., Girirajan, S., et al. (2010). A Large and Complex Structural Polymorphism at 16p12.1 Underlies Microdeletion Disease Risk. *Nat. Genet.* 42, 745–750. doi:10.1038/ng.643

Aybar, M. J., Nieto, M. A., and Mayor, R. (2003). Snail Precedes Slug in the Genetic cascade Required for the Specification and Migration of the Xenopus Neural Crest. *Development* 130, 483–494. doi:10.1242/dev.00238

Bellmeyer, A., Krase, J., Lindgren, J., and LaBonne, C. (2003). The Protooncogene C-Myc Is an Essential Regulator of Neural Crest Formation in xenopus. *Dev. Cel* 4, 827–839. doi:10.1016/s1534-5807(03)00160-6

Blazejewski, S. M., Bennison, S. A., Smith, T. H., and Toyo-Oka, K. (2018). Neurodevelopmental Genetic Diseases Associated with Microdeletions and Microduplications of Chromosome 17p13.3. *Front. Genet.* 9, 80. doi:10.3389/fgene.2018.00080

Camacho-Macorra, C., Sintes, M., Tabanera, N., Grasa, I., Bovolenta, P., and Cardozo, M. J. (2021). Mosmo Is Required for Zebrafish Craniofacial Formation. *Front. Cel Dev. Biol.* 9, 767048. doi:10.3389/fcell.2021.767048

Chen, Y.-C., Chang, Y.-W., and Huang, Y.-S. (2019). Dysregulated Translation in Neurodevelopmental Disorders: An Overview of Autism-Risk Genes Involved in Translation. *Develop Neurobiol.* 79, 60–74. doi:10.1002/dneu.22653

da Costa, M. C., Trentin, A. G., and Calloni, G. W. (2018). FGF8 and Shh Promote the Survival and Maintenance of Multipotent Neural Crest Progenitors. *Mech. Develop.* 154, 251–258. doi:10.1016/j.mod.2018.07.012

del Barrio, M. G., and Nieto, M. A. (2002). Overexpression of Snail Family Members Highlights Their Ability to Promote Chick Neural Crest Formation. *Development* 129, 1583–1593. doi:10.1242/dev.129.7.1583

Deshpande, A., and Weiss, L. A. (2018). Recurrent Reciprocal Copy Number Variants: Roles and Rules in Neurodevelopmental Disorders. *Devel Neurobio* 78, 519–530. doi:10.1002/dneu.22587

Devotta, A., Hong, C. S., and Saint-Jeannet, J. P. (2018). Dkk2 Promotes Neural Crest Specification by Activating Wnt/β-Catenin Signaling in a GSK3β Independent Manner. *Elife* 7. doi:10.7554/eLife.34404

Dickinson, A. J. G. (2016). Using Frogs Faces to Dissect the Mechanisms Underlying Human Orofacial Defects. *Semin. Cel Dev. Biol.* 51, 54–63. doi:10.1016/j.semcdb.2016.01.016

Dubey, A., and Saint-Jeannet, J.-P. (2017). Modeling Human Craniofacial Disorders in Xenopus. *Curr. Pathobiol Rep.* 5, 79–92. doi:10.1007/s40139-017-0128-8

Dworkin, S., Boglev, Y., Owens, H., and Goldie, S. J. (2016). The Role of Sonic Hedgehog in Craniofacial Patterning, Morphogenesis and Cranial Neural Crest Survival. *J. Dev. Biol.* 4. doi:10.3390/jdb4030024

Etchevers, H. C., Dupin, E., and Le Douarin, N. M. (2019). The Diverse Neural Crest: from Embryology to Human Pathology. *Development* 146. doi:10.1242/dev.169821

Everson, J. L., Fink, D. M., Yoon, J. W., Leslie, E. J., Kietzman, H. W., Ansen-Wilson, L. J., et al. (2017). Sonic Hedgehog Regulation of Foxf2 Promotes Cranial Neural Crest Mesenchyme Proliferation and Is Disrupted in Cleft Lip Morphogenesis. *Development* 144, 2082–2091. doi:10.1242/dev.149930

Fish, J. L. (2016). Developmental Mechanisms Underlying Variation in Craniofacial Disease and Evolution. *Dev. Biol.* 415, 188–197. doi:10.1016/j.ydbio.2015.12.019

Gaignard, P., Eyer, D., Lebigot, E., Oliveira, C., Therond, P., Boutron, A., et al. (2017). UQCRC2 Mutation in a Patient with Mitochondrial Complex III Deficiency Causing Recurrent Liver Failure, Lactic Acidosis and Hypoglycemia. *J. Hum. Genet.* 62, 729–731. doi:10.1038/jhg.2017.22

Girirajan, S., Rosenfeld, J. A., Cooper, G. M., Antonacci, F., Siswara, P., Itsara, A., et al. (2010). A Recurrent 16p12.1 Microdeletion Supports a Two-Hit Model for Severe Developmental Delay. *Nat. Genet.* 42, 203–209. doi:10.1038/ng.534

Gonsalvez, D. G., Li-Yuen-Fong, M., Cane, K. N., Stamp, L. A., Young, H. M., and Anderson, C. R. (2015). Different Neural Crest Populations Exhibit Diverse Proliferative Behaviors. *Devel Neurobio* 75, 287–301. doi:10.1002/dneu.22229

Grieco, T. M., and Hlusko, L. J. (2016). Insight from Frogs: Sonic Hedgehog Gene Expression and a Re-evaluation of the Vertebrate Odontogenic Band. *Anat. Rec.* 299, 1099–1109. doi:10.1002/ar.23378

Griffin, J. N., Del Viso, F., Duncan, A. R., Robson, A., Hwang, W., Kulkarni, S., et al. (2018). RAPGEF5 Regulates Nuclear Translocation of β-Catenin. *Dev. Cel* 44, 248–260. doi:10.1016/j.devcel.2017.12.001

Gross, J. B., and Hanken, J. (2008). Segmentation of the Vertebrate Skull: Neural-Crest Derivation of Adult Cartilages in the Clawed Frog, *Xenopus laevis*. *Integr. Comp. Biol.* 48, 681–696. doi:10.1093/icb/icn077

Hammond, N. L., Brookes, K. J., and Dixon, M. J. (2018). Ectopic Hedgehog Signaling Causes Cleft Palate and Defective Osteogenesis. *J. Dent Res.* 97, 1485–1493. doi:10.1177/0022034518785336

Hu, P., Wu, S., Sun, Y., Yuan, C.-C., Kobayashi, R., Myers, M. P., et al. (2002). Characterization of Human RNA Polymerase III Identifies Orthologues for *Saccharomyces cerevisiae* RNA Polymerase III Subunits. *Mol. Cel Biol* 22, 8044–8055. doi:10.1128/mcb.22.22.8044-8055.2002

Hwang, J.-Y., Lee, J., Oh, C.-K., Kang, H. W., Hwang, I.-Y., Um, J. W., et al. (2016). Proteolytic Degradation and Potential Role of Onconeural Protein Cdr2 in Neurodegeneration. *Cell Death Dis* 7, e2240. doi:10.1038/cddis.2016.151

Jensen, M., Kooy, R. F., Simon, T. J., Reyniers, E., Girirajan, S., and Tassone, F. (2018). A Higher Rare CNV burden in the Genetic Background Potentially Contributes to Intellectual Disability Phenotypes in 22q11.2 Deletion Syndrome. *Eur. J. Med. Genet.* 61, 209–212. doi:10.1016/j.ejmg.2017.11.016

Kasherman, M. A., Premarathne, S., Burne, T. H. J., Wood, S. A., and Piper, M. (2020). The Ubiquitin System: a Regulatory Hub for Intellectual Disability and Autism Spectrum Disorder. *Mol. Neurobiol.* doi:10.1007/s12035-020-01881-x

Kerney, R. R., Brittain, A. L., Hall, B. K., and Buchholz, D. R. (2012). Cartilage on the Move: Cartilage Lineage Tracing during Tadpole Metamorphosis. *Develop. Growth Differ.* 54, 739–752. doi:10.1111/dgd.12002

Kirby, R. S. (2017). The Prevalence of Selected Major Birth Defects in the United States. *Semin. Perinatology* 41, 338–344. doi:10.1053/j.semperi.2017.07.004

Kurosaka, H., Iulianella, A., Williams, T., and Trainor, P. A. (2014). Disrupting Hedgehog and WNT Signaling Interactions Promotes Cleft Lip Pathogenesis. *J. Clin. Invest.* 124, 1660–1671. doi:10.1172/jci72688

LaBonne, C., and Bronner-Fraser, M. (1998). Neural Crest Induction in Xenopus: Evidence for a Two-Signal Model. *Development* 125, 2403–2414. doi:10.1242/dev.125.13.2403

LaBonne, C., and Bronner-Fraser, M. (2000). Snail-related Transcriptional Repressors Are Required in Xenopus for Both the Induction of the Neural

Crest and its Subsequent Migration. *Dev. Biol.* 221, 195–205. doi:10.1006/dbio.2000.9609

Lasser, M., Pratt, B., Monahan, C., Kim, S. W., and Lowery, L. A. (2019). The Many Faces of Xenopus: *Xenopus laevis* as a Model System to Study Wolf-Hirschhorn Syndrome. *Front. Physiol.* 10, 817. doi:10.3389/fphys.2019.00817

Lasser, M., Tiber, J., and Lowery, L. A. (2018). The Role of the Microtubule Cytoskeleton in Neurodevelopmental Disorders. *Front. Cel. Neurosci.* 12, 165. doi:10.3389/fncel.2018.00165

Lichtig, H., Artamonov, A., Polevoy, H., Reid, C. D., Bielas, S. L., and Frank, D. (2020). Modeling Bainbridge-Ropers Syndrome in *Xenopus laevis* Embryos. *Front. Physiol.* 11, 75. doi:10.3389/fphys.2020.00075

Mathieu, J., and Ruohola-Baker, H. (2017). Metabolic Remodeling during the Loss and Acquisition of Pluripotency. *Development* 144, 541–551. doi:10.1242/dev.128389

Merkuri, F., and Fish, J. L. (2019). Developmental Processes Regulate Craniofacial Variation in Disease and Evolution. *Genesis* 57, e23249. doi:10.1002/dvg.23249

Millington, G., Elliott, K. H., Chang, Y.-T., Chang, C.-F., Dlugosz, A., and Brugmann, S. A. (2017). Cilia-dependent GLI Processing in Neural Crest Cells Is Required for Tongue Development. *Dev. Biol.* 424, 124–137. doi:10.1016/j.ydbio.2017.02.021

Mills, A., Bearce, E., Cella, R., Kim, S. W., Selig, M., Lee, S., et al. (2019). Wolf-Hirschhorn Syndrome-Associated Genes Are Enriched in Motile Neural Crest Cells and Affect Craniofacial Development in *Xenopus laevis*. *Front. Physiol.* 10, 431. doi:10.3389/fphys.2019.00431

Miyake, N., Yano, S., Sakai, C., Hatakeyama, H., Matsushima, Y., Shiina, M., et al. (2013). Mitochondrial Complex III Deficiency Caused by a HomozygousUQCRC2Mutation Presenting with Neonatal-Onset Recurrent Metabolic Decompensation. *Hum. Mutat.* 34, 446–452. doi:10.1002/humu.22257

Monsoro-Burq, A.-H., Fletcher, R. B., and Harland, R. M. (2003). Neural Crest Induction by Paraxial Mesoderm in Xenopus Embryos Requires FGF Signals. *Development* 130, 3111–3124. doi:10.1242/dev.00531

Nieuwkoop, P. D., and Faber, J. (1994). *Normal Table of Xenopus Laevis (Daudin)*. New York: Garland Publishing Inc.

O'Donovan, K. J., Diedler, J., Couture, G. C., Fak, J. J., and Darnell, R. B. (2010). The Onconeural Antigen Cdr2 Is a Novel APC/C Target that Acts in Mitosis to Regulate C-Myc Target Genes in Mammalian Tumor Cells. *PLoS One* 5, e10045. doi:10.1371/journal.pone.0010045

Okano, H. J., Park, W.-Y., Corradi, J. P., and Darnell, R. B. (1999). The Cytoplasmic Purkinje Onconeural Antigen Cdr2 Down-Regulates C-Myc Function: Implications for Neuronal and Tumor Cell Survival. *Genes Develop.* 13, 2087–2097. doi:10.1101/gad.13.16.2087

Okuhara, S., Birjandi, A. A., Adel Al-Lami, H., Sagai, T., Amano, T., Shiroishi, T., et al. (2019). Temporospatial Sonic Hedgehog Signalling Is Essential for Neural Crest-dependent Patterning of the Intrinsic Tongue Musculature. *Development* 146. doi:10.1242/dev.180075

Perestrelo, T., Correia, M., Ramalho-Santos, J., and Wirtz, D. (2018). Metabolic and Mechanical Cues Regulating Pluripotent Stem Cell Fate. *Trends Cel Biol.* 28, 1014–1029. doi:10.1016/j.tcb.2018.09.005

Pizzo, L., Jensen, M., Polyak, A., Rosenfeld, J. A., Mannik, K., Krishnan, A., et al. (2019). Rare Variants in the Genetic Background Modulate Cognitive and Developmental Phenotypes in Individuals Carrying Disease-Associated Variants. *Genet. Med.* 21, 816–825. doi:10.1038/s41436-018-0266-3

Pizzo, L., Lasser, M., Yusuff, T., Jensen, M., Ingraham, P., Huber, E., et al. (2021). Functional Assessment of the "Two-Hit" Model for Neurodevelopmental Defects in Drosophila and *X. laevis*. *Plos Genet.* 17, e1009112. doi:10.1371/journal.pgen.1009112

Pla, P., and Monsoro-Burq, A. H. (2018). The Neural Border: Induction, Specification and Maturation of the Territory that Generates Neural Crest Cells. *Dev. Biol.* 444 (Suppl. 1), S36–S46. doi:10.1016/j.ydbio.2018.05.018

Prasad, M. S., Charney, R. M., and García-Castro, M. I. (2019). Specification and Formation of the Neural Crest: Perspectives on Lineage Segregation. *Genesis* 57, e23276. doi:10.1002/dvg.23276

Pusapati, G. V., Kong, J. H., Patel, B. B., Krishnan, A., Sagner, A., Kinnebrew, M., et al. (2018). CRISPR Screens Uncover Genes that Regulate Target Cell Sensitivity to the Morphogen Sonic Hedgehog. *Dev. Cel* 44, 113–129. doi:10.1016/j.devcel.2017.12.003

Rajan, S. G., Gallik, K. L., Monaghan, J. R., Uribe, R. A., Bronner, M. E., and Saxena, A. (2018). Tracking Neural Crest Cell Cycle Progression *In Vivo*. *Genesis* 56, e23214. doi:10.1002/dvg.23214

Rogers, C. D., and Nie, S. (2018). *Specifying Neural Crest Cells: From Chromatin to Morphogens and Factors in between*. Wiley Interdiscip Rev Dev Biol, e322.

Rutherford, E. L., and Lowery, L. A. (2016). Exploring the Developmental Mechanisms Underlying Wolf-Hirschhorn Syndrome: Evidence for Defects in Neural Crest Cell Migration. *Dev. Biol.* 420, 1–10. doi:10.1016/j.ydbio.2016.10.012

Rylaarsdam, L., and Guemez-Gamboa, A. (2019). Genetic Causes and Modifiers of Autism Spectrum Disorder. *Front. Cel. Neurosci.* 13, 385. doi:10.3389/fncel.2019.00385

Schindelin, J., Arganda-Carreras, I., Frise, E., Kaynig, V., Longair, M., Pietzsch, T., et al. (2012). Fiji: an Open-Source Platform for Biological-Image Analysis. *Nat. Methods* 9, 676–682. doi:10.1038/nmeth.2019

Schubert, M., Panja, D., Haugen, M., Bramham, C. R., and Vedeler, C. A. (2014). Paraneoplastic CDR2 and CDR2L Antibodies Affect Purkinje Cell Calcium Homeostasis. *Acta Neuropathol.* 128, 835–852. doi:10.1007/s00401-014-1351-6

Schwenty-Lara, J., Nehl, D., and Borchers, A. (2020). The Histone Methyltransferase KMT2D, Mutated in Kabuki Syndrome Patients, Is Required for Neural Crest Cell Formation and Migration. *Hum. Mol. Genet.* 29, 305–319. doi:10.1093/hmg/ddz284

Shan, W., Li, J., Xu, W., Li, H., and Zuo, Z. (2019). Critical Role of UQCRC1 in Embryo Survival, Brain Ischemic Tolerance and normal Cognition in Mice. *Cell. Mol. Life Sci.* 76, 1381–1396. doi:10.1007/s00018-019-03007-6

Shang, Y., Zhang, F., Li, D., Li, C., Li, H., Jiang, Y., et al. (2018). Overexpression of UQCRC2 Is Correlated with Tumor Progression and Poor Prognosis in Colorectal Cancer. *Pathol. - Res. Pract.* 214, 1613–1620. doi:10.1016/j.prp.2018.08.012

Sierra-Arregui, T., Llorente, J., Gimenez Minguez, P., Tonnesen, J., and Penagarikano, O. (2020). Neurobiological Mechanisms of Autism Spectrum Disorder and Epilepsy, Insights from Animal Models. *Neuroscience*. doi:10.1016/j.neuroscience.2020.02.043

Singh, M. D., Jensen, M., Lasser, M., Huber, E., Yusuff, T., Pizzo, L., et al. (2020). NCBP2 Modulates Neurodevelopmental Defects of the 3q29 Deletion in Drosophila and *Xenopus laevis* Models. *Plos Genet.* 16, e1008590. doi:10.1371/journal.pgen.1008590

Sive, H. L., Grainger, R. M., and Harland, R. M. (2007). Baskets for *In Situ* Hybridization and Immunohistochemistry. *CSH Protoc.* 2007. pdb prot4777.

Sive, H. L., Grainger, R. M., and Harland, R. M. (2010). Microinjection of Xenopus Embryos. *Cold Spring Harbor Protoc.* 2010, pdb ip81. doi:10.1101/pdb.ip81

Sperber, H., Mathieu, J., Wang, Y., Ferreccio, A., Hesson, J., Xu, Z., et al. (2015). The Metabolome Regulates the Epigenetic Landscape during Naive-To-Primed Human Embryonic Stem Cell Transition. *Nat. Cel Biol* 17, 1523–1535. doi:10.1038/ncb3264

Spokony, R. F., Aoki, Y., Saint-Germain, N., Magner-Fink, E., and Saint-Jeannet, J.-P. (2002). The Transcription Factor Sox9 Is Required for Cranial Neural Crest Development inXenopus. *Development* 129, 421–432. doi:10.1242/dev.129.2.421

Szabó, A., and Mayor, R. (2018). Mechanisms of Neural Crest Migration. *Annu. Rev. Genet.* 52, 43–63. doi:10.1146/annurev-genet-120417-031559

Tahir, R., Kennedy, A., Elsea, S. H., and Dickinson, A. J. (2014). Retinoic Acid Induced-1 (Rai1) Regulates Craniofacial and Brain Development in Xenopus. *Mech. Develop.* 133, 91–104. doi:10.1016/j.mod.2014.05.004

Theveneau, E., and Mayor, R. (2012). Neural Crest Delamination and Migration: from Epithelium-To-Mesenchyme Transition to Collective Cell Migration. *Dev. Biol.* 366, 34–54. doi:10.1016/j.ydbio.2011.12.041

Tinevez, J.-Y., Perry, N., Schindelin, J., Hoopes, G. M., Reynolds, G. D., Laplantine, E., et al. (2017). TrackMate: An Open and Extensible Platform for Single-Particle Tracking. *Methods* 115, 80–90. doi:10.1016/j.ymeth.2016.09.016

Trainor, P. A. (2010). Craniofacial Birth Defects: The Role of Neural Crest Cells in the Etiology and Pathogenesis of Treacher Collins Syndrome and the Potential for Prevention. *Am. J. Med. Genet.* 152A, 2984–2994. doi:10.1002/ajmg.a.33454

Van Otterloo, E., Williams, T., and Artinger, K. B. (2016). The Old and New Face of Craniofacial Research: How Animal Models Inform Human Craniofacial Genetic and Clinical Data. *Dev. Biol.* 415, 171–187. doi:10.1016/j.ydbio.2016.01.017

Vega-Lopez, G. A., Cerrizuela, S., Tribulo, C., and Aybar, M. J. (2018). Neurocristopathies: New Insights 150 Years after the Neural Crest Discovery. *Dev. Biol.* 444 (Suppl. 1), S110–S143. doi:10.1016/j.ydbio.2018.05.013

Venkatraman, A., and Opal, P. (2016). Paraneoplastic Cerebellar Degeneration with Anti-yo Antibodies - a Review. *Ann. Clin. Transl Neurol.* 3, 655–663. doi:10.1002/acn3.328

Villanueva, S., Glavic, A., Ruiz, P., and Mayor, R. (2002). Posteriorization by FGF, Wnt, and Retinoic Acid Is Required for Neural Crest Induction. *Dev. Biol.* 241, 289–301. doi:10.1006/dbio.2001.0485

Wang, Q., Kurosaka, H., Kikuchi, M., Nakaya, A., Trainor, P. A., and Yamashiro, T. (2019). Perturbed Development of Cranial Neural Crest Cells in Association with Reduced Sonic Hedgehog Signaling Underlies the Pathogenesis of Retinoic-Acid-Induced Cleft Palate. *Dis. Model. Mech.* 12. doi:10.1242/dmm.040279

Wu, J., Yang, J., and Klein, P. S. (2005). Neural Crest Induction by the Canonical Wnt Pathway Can Be Dissociated from Anterior-Posterior Neural Patterning in Xenopus. *Dev. Biol.* 279, 220–232. doi:10.1016/j.ydbio.2004.12.016

Conflict of Interest: The authors declare that the research was conducted in the absence of any commercial or financial relationships that could be construed as a potential conflict of interest.